

Density Functional Theory Study on Defect Behavior Related to the Bulk Lifetime of Silicon Crystals for Power Device Application

Daiki Tsuchiya, Koji Sueoka, and Hidekazu Yamamoto*

Among the insulated-gate bipolar transistors (IGBTs) and PIN junction diodes, there are devices that the recombination centers, namely lifetime-control defects, are introduced into phosphorus (P) doped n-type silicon (Si) crystals by electron beam irradiation. The lifetime-control defects are considered as they form deep levels such as the vacancy–vacancy (V–V) pair and vacancy–phosphorus (V–P) pair. In the case of using Czochralski Si wafers, it is considered that some pairs of carbon (C), oxygen (O), and their complexes are believed to have a negative impact to the lifetime-control defects. In this study, density functional theory (DFT) calculations are performed to understand the formation behavior of lifetime-control defects and the formation behavior of complexes composed of C and O atoms believed to interact with lifetime-control defects. On the basis of these results, DFT calculations related to the structural change of lifetime-control defects are performed. The most important result is that instead of the interstitial carbon–substitutional carbon (C_i – C_s) pair, the interstitial C_i atom and interstitial carbon–interstitial oxygen (C_i – O_i) pair are the strong candidates to affect controllability of lifetime by interacting with V composed of lifetime-control defects.

The most serious problem is that the lifetime is extended by the structural changes of lifetime-control defects during a power supply operation.^[1,2] However, the mechanism that causes the structural changes is still unknown.

Lifetime-control defects are considered as they form deep levels such as a vacancy–vacancy (V–V) pair and vacancy–phosphorus (V–P) pair.^[3–7] In the case of using Czochralski (CZ) Si wafers, interstitial carbon (C_i) atoms are formed by the reaction of substitutional carbon (C_s) and a self-interstitial (I), and interstitial carbon–substitutional carbon (C_i – C_s) pairs and interstitial carbon–interstitial oxygen (C_i – O_i) pairs are believed to have a negative impact to the lifetime-control defects (V–V pair and V–P pair).^[8–11] C_i atom is easily expected to be a candidate to affect controllability of lifetime by interacting with V. However, it is not still clear whether C_i – C_s pair and C_i – O_i pair affect the lifetime controllability.

In this study, density functional theory (DFT) calculations were performed to understand 1) the formation behavior of lifetime-control defects such as V–V and V–P pairs and 2) the formation behavior of complexes composed of C and O atoms believed to interact with lifetime-control defects. On the basis of these results, we performed calculations related to the structural changes of lifetime-control defects; the interaction of the candidate complexes, found by (1) and (2), with V or P composed of lifetime-control defects. As it will be cited and compared in this paper, a number of DFT calculations have been performed for the various defects related to vacancy, phosphorous, oxygen and carbon etc in Si crystals.^[5,7,11–30] However, from the viewpoint of the influence on lifetime control defects, systematic calculations have not been reported to clarify the candidates to affect the lifetime-control defects. Especially, as far as to our knowledge, the binding energies (E_b) of V – C_i – O_i , P – C_i – O_i , V – C_i – C_s , and P – C_i – C_s have not been reported yet.

A notable feature of this research is that the most stable and metastable structures were obtained without omission by calculating the E_b between reactive species by considering all the possible atomic configurations in a Si 64-atom cubic

1. Introduction

To achieve a low-carbon society, reducing the number of loss of power devices is an urgent problem that needs to be solved. An essential factor to achieve low-loss insulated-gate bipolar transistors (IGBTs) is controlling the bulk lifetime of phosphorus (P) doped n-type silicon (Si) crystals. Among the IGBTs and PIN junction diodes, there are devices that the recombination centers, namely lifetime-control defects, are introduced into such crystals by electron beam irradiation.^[1,2]

D. Tsuchiya, Prof. K. Sueoka
Okayama Prefectural University
111 Kuboki, Soja, Okayama 719-1197, Japan
E-mail: cd30022h@c.oka-pu.ac.jp

Prof. H. Yamamoto
Chiba Institute of Technology
2-17-1 Tsudanuma, Narashino, Chiba 275-0016, Japan

 The ORCID identification number(s) for the author(s) of this article can be found under <https://doi.org/10.1002/pssa.201800615>.

DOI: 10.1002/pssa.201800615

cell.^[18,19,31] This approach provided us with the reaction path to form complexes during each reaction.

2. Calculation Details

The DFT calculations in this study are based on a standard approach, using a local density approximation with ultrasoft pseudopotentials and plane waves as a basis set for efficiently optimizing the atomic structure.^[32] A generalized gradient approximation (GGA) was used for the exchange-correlation term, and the functional form was of the Perdew-Burke-Ernzerhof (PBE) type.^[33] The cutoff energy used for the plane-wave expansion was 340 eV. The Cambridge Serial Total Energy Package (CASTEP) code is used to self-consistently solve the Kohn-Sham equation under a three-dimensional periodic boundary condition.^[34] The density mixing method was used to minimize the energy of the electronic system, and the Broyden-Fletcher-Goldfarb-Shanno (BFGS) structural optimization method was used to optimize atom placement.^[35,36] As for the convergence condition used in the electronic-state calculation, the total energy change was less than 5.0×10^{-7} eV/atom, and in geometry optimization, the total energy change was less than 5.0×10^{-6} eV/atom, an atomic displacement less than 5.0×10^{-4} Å, an atomic force less than 0.01 eV Å⁻¹, and stress in the cell less than 0.02 GPa. We carried out k-point sampling at $2 \times 2 \times 2$ special points in a Monkhorst-Pack grid, which was sufficient to obtain converged results for the Si 64-atom supercells.^[37] A Si 64-atom cubic cell with a cell size of 10.937 Å, namely a $2 \times 2 \times 2$ supercell constructed with a conventional cell, was used. The cell was surrounded by (100), (010), and (001) planes, and each edge of the cell was along the [100], [010], and [001] directions. Three-dimensional periodic boundary conditions were set for each calculation model. A Si 216-atom cubic cell with a cell size of 16.392 Å, namely a $3 \times 3 \times 3$ supercell constructed with a conventional cell, was also used to obtain the more reliable E_b of the most stable complexes.

In the present work, the calculation cells were kept electronically neutral. That is, only the uncharged state is considered, while the direct exchange of electrons between two reactants in the cell is automatically taken into account. The impact of charge states will be considered in the future study.

We handled the following behaviors related to the lifetime-control defects:

- 1) Formation behavior of lifetime-control defects such as V–V and V–P.
- 2) Formation behavior of complexes believed to interact with lifetime-control defects.
- 3) Structural change of lifetime-control defects.

Considering that the target region is the P doped n-type CZ-Si crystals with electron beam irradiation, some of the intrinsic point defects (vacancy V and self-interstitial I), dopant (P) atom, and impurity (C and O) atoms were introduced in a cubic cell. Total energy (E_{tot}) of the cell was calculated on the basis of the DFT calculation. A notable feature of this

research is that we considered all possible atomic configurations in a Si 64-atom cubic cell. This brought about the most stable and metastable structures of target complexes and the formation path of stable complexes. The calculation model used in each reaction, its initial configuration, and calculation method of binding energy are described in Sections 2.1 to 2.3.

2.1. Formation Behavior of Lifetime-Control Defects Such As V–V and V–P

In a Si 64-atom cubic cell, there are sites (1st to 9th) from a center atom as shown in Figure 1. In the calculation, a Vor P atom was placed at the center (in red) and the other V was arranged from the 1st to 9th sites (in blue). The binding energy (E_b) of V and V, and of V and P are calculated with Equations (1) and (2), respectively, as

$$\begin{aligned} E_b(V, V) = & \{E_{tot}[\text{Si}_{63}V_1] + E_{tot}[\text{Si}_{63}V_1]\} \\ & - \{E_{tot}[\text{Si}_{62}V_2] + E_{tot}[\text{Si}_{64}]\} \end{aligned} \quad (1)$$

$$\begin{aligned} E_b(V, P) = & \{E_{tot}[\text{Si}_{63}V_1] + E_{tot}[\text{Si}_{63}P_1]\} \\ & - \{E_{tot}[\text{Si}_{62}V_1P_1] + E_{tot}[\text{Si}_{64}]\} \end{aligned} \quad (2)$$

2.2. Formation Behavior of Complexes Believed to Interact With Lifetime-Control Defects

It is known that I is most stable at the [110] dumbbell (D)-site in a perfect Si crystal.^[5] In the calculation for the reaction of C and I, a substitutional carbon (C_s) atom was arranged around an I. By considering the symmetry of the diamond structure, there are 36 independent models as shown in Figure 2(a). In addition to these

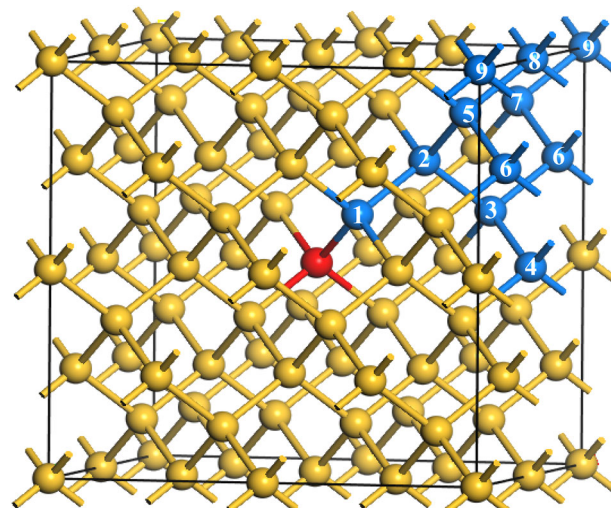


Figure 1. Si 64-atom cubic cell: 1st to 9th site (in blue) from a center atom (in red).

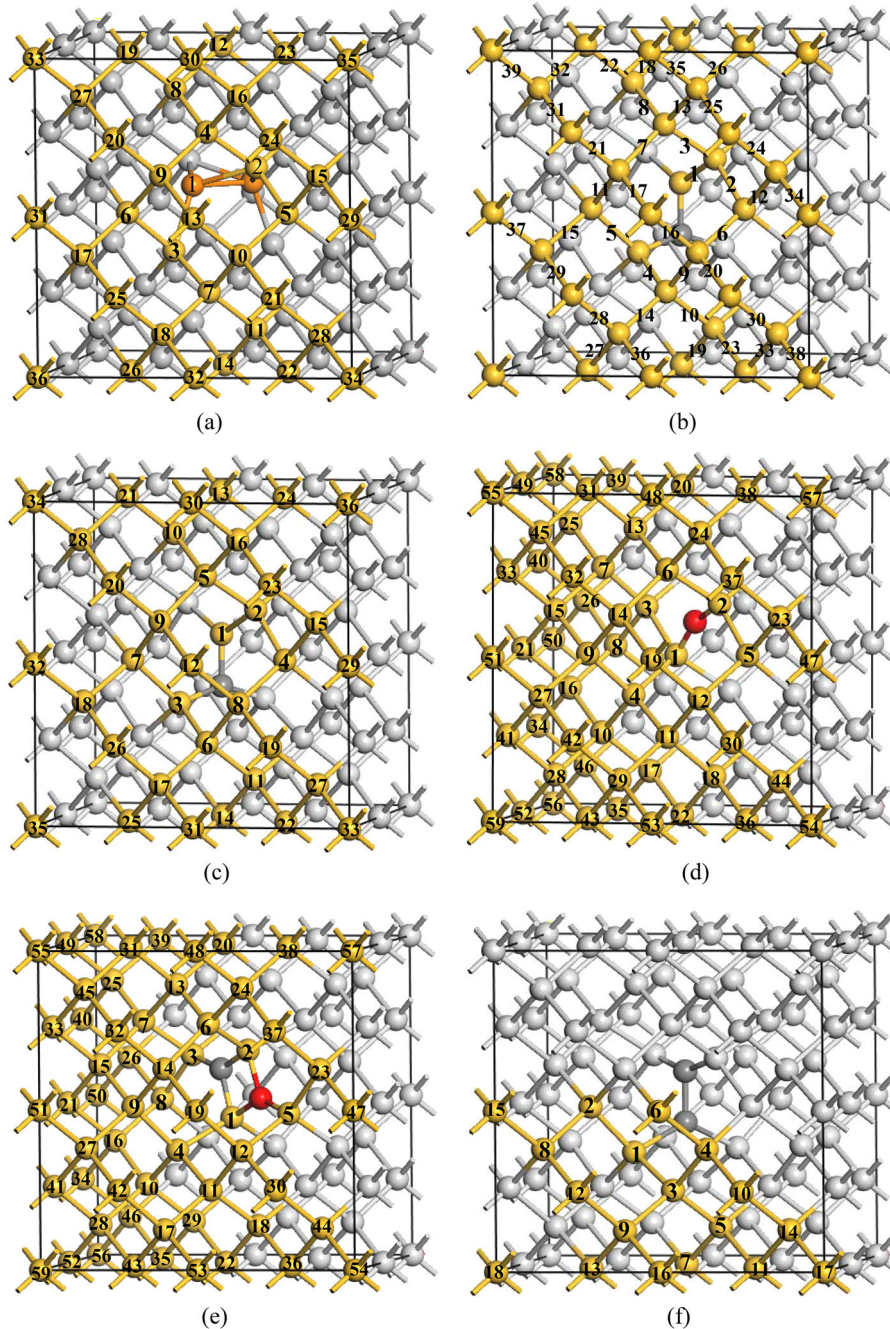


Figure 2. Initial configurations in Si 64-atom cubic cell. a) I (in orange) and site of C_s; b) C_i (in gray) and site of O_i; c) C_i (in gray) and site of C_s, V, P; d) O_i (in red) and site of V, P; e) C_i-O_i (in gray and red) and site of V, P; and f) C_i-C_s (in gray) and site of V, P.

models, we considered [100] D-site composed of I and C_s atoms as the model No. 0. E_b of I and C_s was calculated with Equation (3) as

$$E_b(I, C_s) = \{E_{tot}[\text{Si}_{64}I_1] + E_{tot}[\text{Si}_{63}C_{s1}]\} - \{E_{tot}[\text{Si}_{63}I_1C_{s1}] + E_{tot}[\text{Si}_{64}]\} \quad (3)$$

Interstitial carbon (C_i) and interstitial oxygen (O_i) atoms are most stable at the [100] D-site and bond center

(B)-site, respectively, in a perfect Si crystal.^[5,20] In the calculation for the reaction of C_i and O_i, an O_i atom was arranged around a C_i atom. By considering the symmetry of the diamond structure, there are 39 independent models as shown in Figure 2(b). E_b of C_i and O_i was calculated with Equation (4) as

$$E_b(C_i, O_i) = \{E_{tot}[\text{Si}_{64}C_{i1}] + E_{tot}[\text{Si}_{64}O_{i1}]\} - \{E_{tot}[\text{Si}_{64}C_{i1}O_{i1}] + E_{tot}[\text{Si}_{64}]\} \quad (4)$$

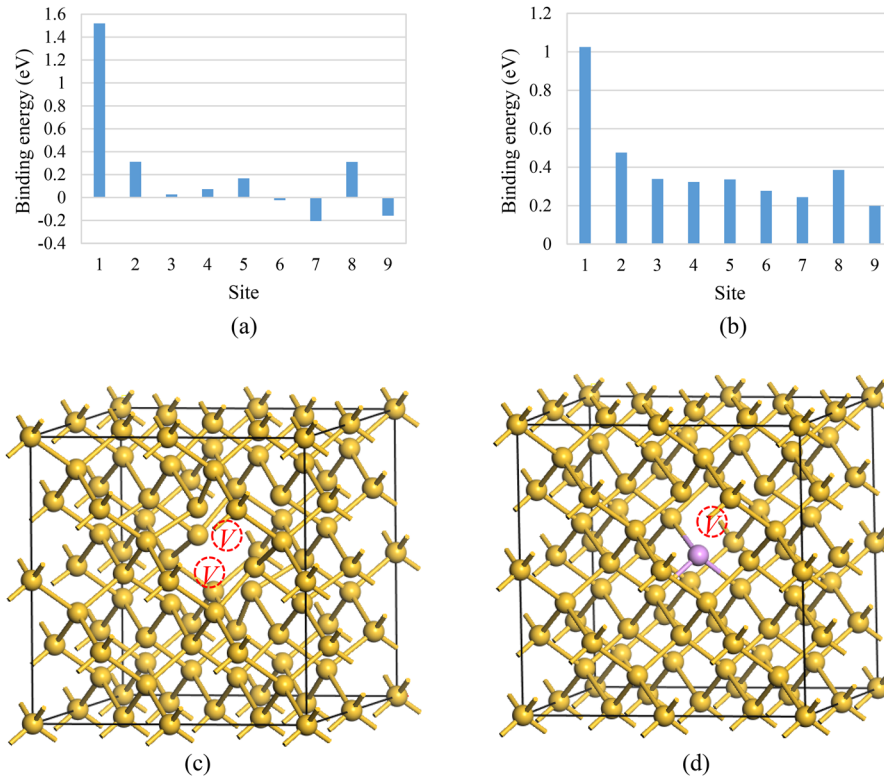


Figure 3. Calculation results about reaction of V and V, V and P. a) Dependence of E_b on V site from the other V; b) dependence of E_b on V site from P; c) most stable structure of V–V (No. 1); and d) most stable structure of V–P (No. 1) (purple sphere indicates P atom).

In the calculation for the reaction of C_i and C_s , a C_s atom was arranged around a C_i atom. There are 36 independent models as shown in Figure 2(c). E_b of C_i and C_s was calculated with Equation (5) as

$$E_b(C_i, C_s) = \{E_{tot}[Si_{63}C_{i1}] + E_{tot}[Si_{64}C_{s1}]\} - \{E_{tot}[Si_{63}C_{i1}C_{s1}] + E_{tot}[Si_{64}]\} \quad (5)$$

2.3. Structural Change of Lifetime-Control Defects

In the calculation for the reaction of V and C_i and of P and C_i , V or P was placed at the substitutional site around a C_i atom. There are 36 independent models as shown in Figure 2(c). E_b of V and C_i and of P and C_i were calculated with Equations (6) and (7) as

$$E_b(V, C_i) = \{E_{tot}[Si_{63}V_1] + E_{tot}[Si_{64}C_{i1}]\} - \{E_{tot}[Si_{63}V_1C_{i1}] + E_{tot}[Si_{64}]\} \quad (6)$$

$$E_b(P, C_i) = \{E_{tot}[Si_{63}P_1] + E_{tot}[Si_{64}C_{i1}]\} - \{E_{tot}[Si_{63}P_1C_{i1}] + E_{tot}[Si_{64}]\} \quad (7)$$

In the calculation for the reaction of V (P) and O_i , V (P) was placed at the substitutional site around an O_i atom.

There are 59 independent models as shown in Figure 2(d). E_b of V and O_i and of P and O_i are calculated with Equations (8) and (9) as

$$E_b(V, O_i) = \{E_{tot}[Si_{63}V_1] + E_{tot}[Si_{64}O_{i1}]\} - \{E_{tot}[Si_{63}V_1O_{i1}] + E_{tot}[Si_{64}]\} \quad (8)$$

$$E_b(P, O_i) = \{E_{tot}[Si_{63}P_1] + E_{tot}[Si_{64}O_{i1}]\} - \{E_{tot}[Si_{63}P_1O_{i1}] + E_{tot}[Si_{64}]\} \quad (9)$$

The C_i-O_i pair is known to be the most stable structure as shown in Figure 2(e).^[11] In the calculation for the reaction of V (P) and C_i-O_i , V (P) was placed at the substitutional site around C_i-O_i pair. There are 59 independent models as shown in Figure 2(e). E_b of V and C_i-O_i and of P and C_i-O_i are calculated with Equations (10) and (11) as

$$E_b(V, C_iO_i) = \{E_{tot}[Si_{63}V_1] + E_{tot}[Si_{64}C_{i1}O_{i1}]\} - \{E_{tot}[Si_{63}V_1C_{i1}O_{i1}] + E_{tot}[Si_{64}]\} \quad (10)$$

$$E_b(P, C_iO_i) = \{E_{tot}[Si_{63}P_1] + E_{tot}[Si_{64}C_{i1}O_{i1}]\} - \{E_{tot}[Si_{63}P_1C_{i1}O_{i1}] + E_{tot}[Si_{64}]\} \quad (11)$$

The most stable C_i-C_s pair obtained is the [100] dumbbell. This structure has been demonstrated only by DFT

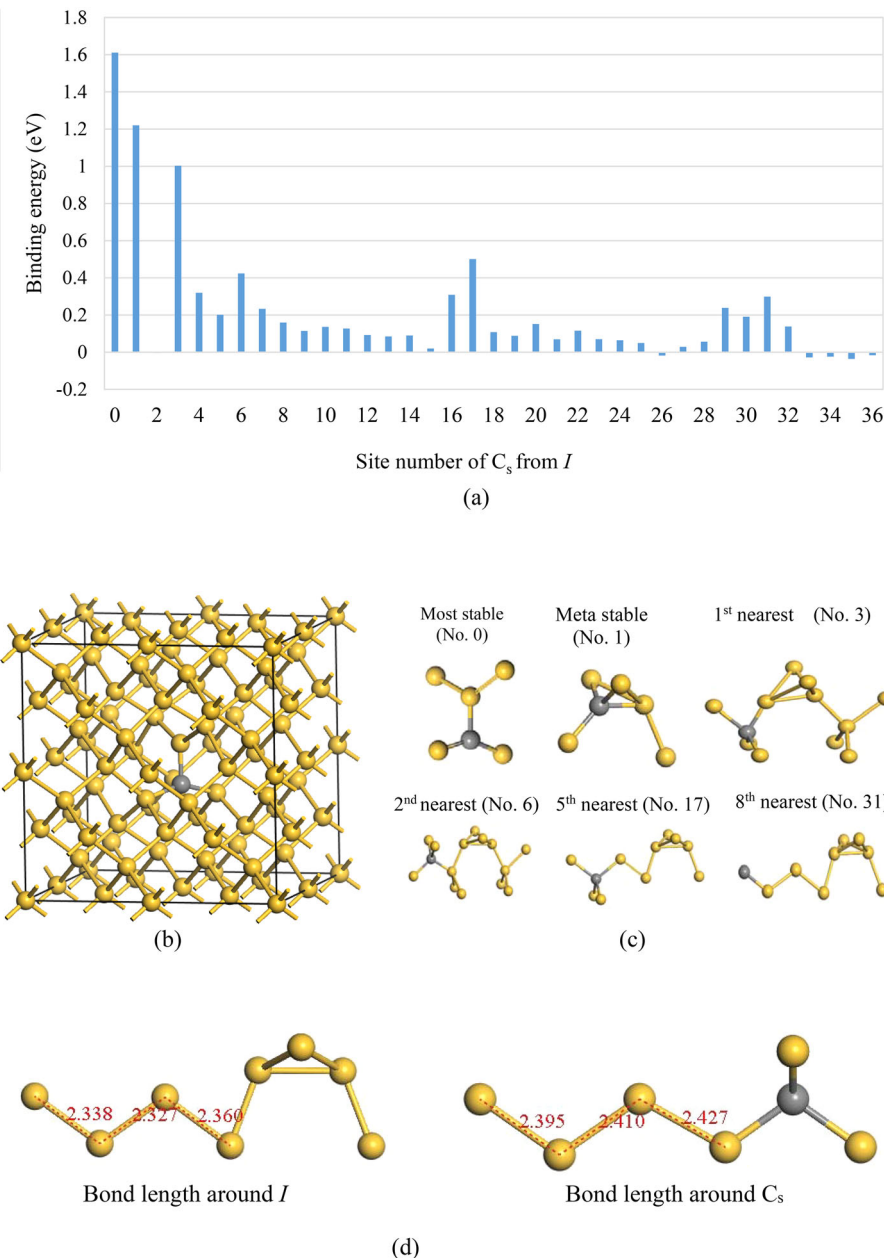


Figure 4. Calculation results about reaction of I and C_s . a) Dependence of E_b on the number of C_s sites from I ; b) most stable structure (No. 0) (gray sphere indicates I atom); c) most stable and metastable structures; and d) bond length around I (left) and C_s (right).

calculations.^[19,21] V or P atom were placed at substitutional site around C_i-C_s pair. There are 18 independent models as shown in Figure 2(f). E_b of V and C_i-C_s , and of P and C_i-C_s are calculated with Equations (12) and (13) as

$$\begin{aligned} E_b(V, C_i C_s) = & \{E_{tot}[Si_{63}V_1] + E_{tot}[Si_{63}C_{i1}C_{s1}]\} \\ & - \{E_{tot}[Si_{62}V_1C_{i1}C_{s1}] + E_{tot}[Si_{64}]\} \end{aligned} \quad (12)$$

$$\begin{aligned} E_b(P, C_i C_s) = & \{E_{tot}[Si_{63}P_1] + E_{tot}[Si_{63}C_{i1}C_{s1}]\} \\ & - \{E_{tot}[Si_{62}P_1C_{i1}C_{s1}] + E_{tot}[Si_{64}]\} \end{aligned} \quad (13)$$

3. Results and Discussion

3.1. Formation Behavior of Lifetime-Control Defect Such As V–V and V–P

Figure 3(a) and (b) show the calculated dependence of E_b on the number of V sites from the other V and P atom, respectively. From Figure 3(a), the most stable V–V pair (Figure 3c) is composed of a V existing at the 1st nearest neighbor site from the other V. At the 2nd neighbor site of the other V, E_b is much less than that at the 1st neighbor site. That is, the impact of a V on the other V stays in the 1st neighbor site.^[7] This is due to the extinction of two dangling bonds when two vacancies

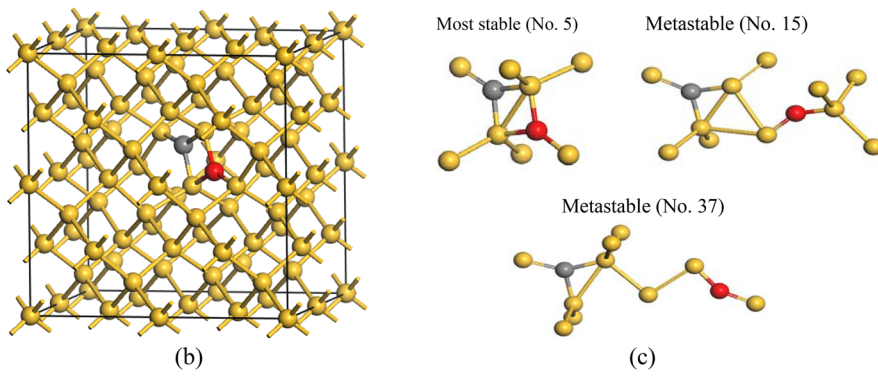
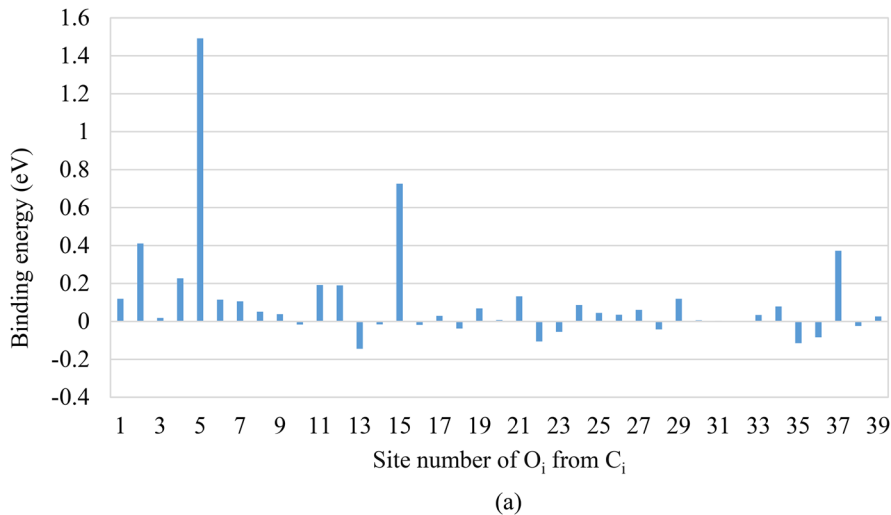


Figure 5. Calculation results about reaction of C_i and O_i . a) Dependence of E_b of C_i-O_i on the number of O_i sites from the C_i atom; b) most stable structure (no. 5) (gray/red sphere indicates C/O atom); c) most stable and metastable structures; and d) bond length around O_i .

form an adjacent V–V pair. E_b of V and P is also the largest when both V and P stay at the 1st neighbor site (Figure 3d). However, as shown in Figure 3(b), the value of E_b is still positive even at the farthest (9th) site ($E_b=0.2$ eV). This result indicates that the influence of P atom on V extends beyond the cell size, which is due to the long-range electrical interaction.^[18]

3.2. Formation Behavior of Complex Interacting Lifetime-Control Defects

3.2.1. Reaction of C_s and I

Figure 4(a) shows the calculated dependence of E_b on the number of C_s sites from I. In the reaction of I and C_s , [100]

D-site composed of I and C atoms is the most stable as shown in Figure 4(b).^[5] That is, I interacts with C_s , which results in the formation of C_i . Some metastable structures are determined as shown in Figure 4(c). C_s and I are stable

Table 1. Bond length around C_i dumbbell.

	Direction A		Direction B	
	Connected with Si atom [Å]	Connected with C atom [Å]	Connected with Si atom [Å]	Connected with C atom [Å]
1st–2nd	2.372	2.479	2.342	2.327
2nd–5th	2.374	2.442	2.335	2.341
5th–8th	2.368	2.415	2.346	2.350

Bond length of Si-Si: 2.368 Å.

on each other's Si-Si zigzag bond. The length of Si-Si bondings in a perfect crystal is 2.368 Å. As shown in Figure 4(d), the decreased bond length around I indicates the occurrence of compressive strain, while the increased bond length around C_s atoms indicates the occurrence of tensile strain. The compensation of strains caused by I and C_s is the reason for the stable C_s - I pair. In the reaction of I and C_s , I moves to C_s atoms along the [110] direction through the metastable structures and forms C_i by the reaction of $I + C_s \rightarrow C_i$.

3.2.2. Reaction of C_i and O_i

Figure 5(a) shows the calculated dependence of E_b of C_i - O_i on the number of O_i sites from the C_i atom. As shown in Figure 5(b), both C_i and O_i atoms bond to three Si ligand atoms and share two of them. Some metastable structures are shown in Figure 5(c). C_i and O_i atoms are stable on each other's zigzag bond. As shown in Figure 5(d), compressive strain occurs on the zigzag bond including O_i atom. The calculated bond lengths of <110> zigzag bonds in the vertical direction of

[100] C_i dumbbell (direction A) and <110> zigzag bonds in the direction of angle of 45 degrees from [100] C_i dumbbell (direction B) are summarized in Table 1. C_i dumbbell causes tensile strain in the direction A and compressive strain in the direction B. By considering the local strain formed by C_i and O_i atoms, C_i and O_i approach each other from the direction A and form a C_i - O_i complex with rhombic structure by the reaction of $C_i + O_i \rightarrow C_i\text{-}O_i$.

3.2.3. Reaction of C_i and C_s

Figure 6(a) shows the calculated dependence of E_b on the number of C_s sites from the C_i atom. The determined most stable structure and some metastable structures are shown in Figure 6(b) and (c), respectively.^[10] At sites No. 1, C_i and C_s atoms form [100] dumbbell, which is the most stable structure. The structure of [100] dumbbell is described as a C_i - C_s defect. As described in the Section 3.2.2, the C_i atom causes compressive strain in the direction B. Therefore, the tensile strain of C_s is probably relaxed to form a C_i - C_s defect.

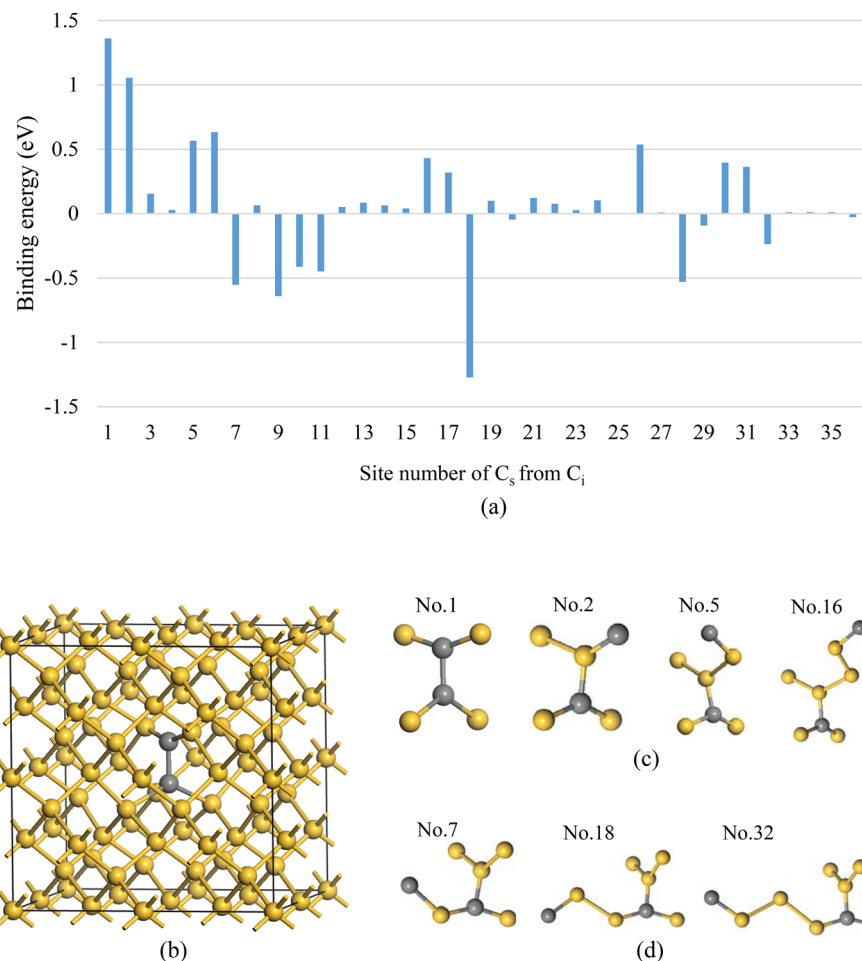


Figure 6. Calculation results about reaction of C_i and C_s . a) Dependence of E_b on the number of C_s sites from the C_i atom; b) most stable structure (No. 1) (gray sphere indicates C atom); c) most stable and metastable structures; and d) unstable structures.

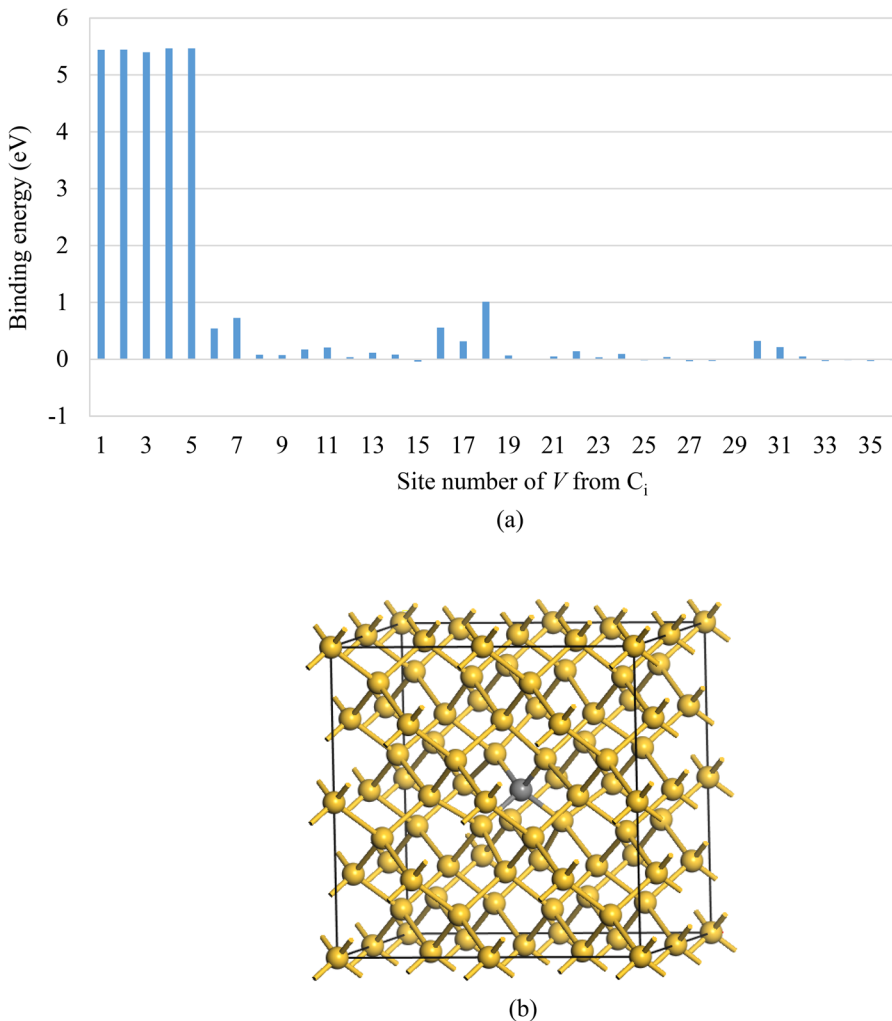


Figure 7. Calculation results about reaction of V and C_i . a) Dependence of E_b on the number of V sites from the C_i atom and b) most stable structure (from No. 1 to No. 5) (gray sphere indicates C atom).

3.3. Structural Change of Lifetime Control Defect

3.3.1. Reaction of V and C_i

Figure 7(a) shows the calculated dependence of E_b on the number of V sites from the C_i atom. The determined most stable structure is shown in **Figure 7(b)**. V and the C_i atom are annihilated and becomes a C_s atom, that is, a substitutional C_s atom is formed by the reaction of $V + C_i \rightarrow C_s$. V is stable on the Si–Si bond in the direction B of the [100] C_i dumbbell because of the compressive strain caused by C_i . V and the C_i atom should approach each other in the direction B of [100] C_i dumbbell.

3.3.2. Reaction of P and C_i

Figure 8(a) shows the calculated dependence of E_b on the number of P sites from the C_i atom. The most stable structure determined is shown in **Figure 8(b)**. P and C_i atoms

form the slightly distorted [100] dumbbell. Some metastable structures are shown in **Figure 8(c)**. Since P atom is slightly smaller than Si atom, C_i atom should approach to P atom in the direction B of [100] C_i dumbbell. By using the Deep Level Transient Spectroscopy method, substitutional phosphorus-interstitial carbon pair ($P-C_i$) was observed at the same time when C_i disappears around room temperature.^[24] The $P-C_i$ complexes have several (at least four) metastable structures which are probably reproduced by the present calculations.^[38–40]

3.3.3. Reaction of V and O_i

Figure 9(a) shows the calculated dependence of E_b on the number of V sites from the O_i atom. V and the O_i atom form a stable complex as shown in **Figure 9(b)**, and are stable on each other's zigzag bond. In the most stable structure, the O_i atom binds with two dangling bonds of V . The O_i atom is displaced in the direction to V as shown in **Figure 9(c)**.^[20]

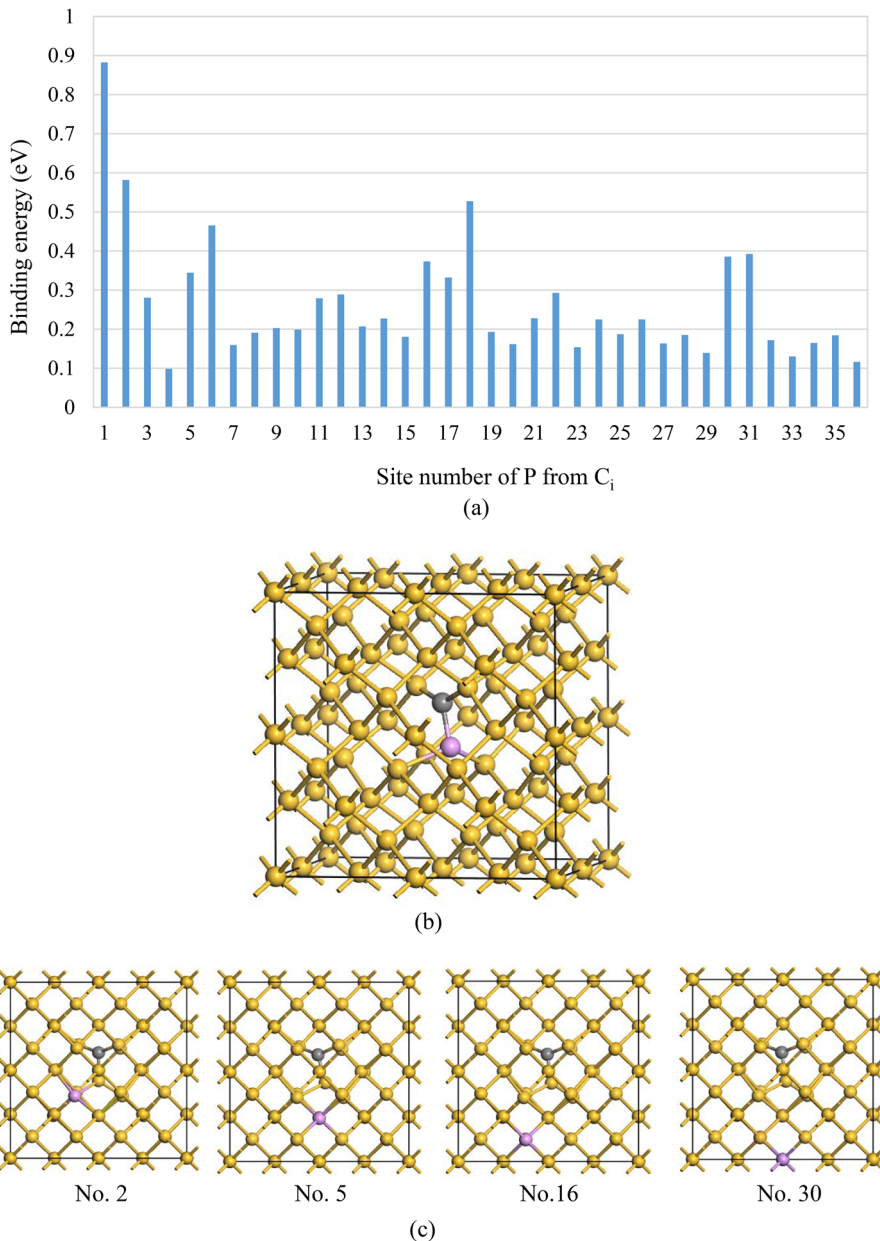


Figure 8. Calculation results about reaction of P and C_i . a) Dependence of E_b on the number of P sites from the C_i atom; b) most stable structure (No. 1) (gray/purple sphere indicates C/P atom); and c) several metastable structures.

3.3.4. Reaction of P and O_i

Figure 10(a) shows the calculated dependence of E_b on the number of P sites from the O_i atom. The most stable structure determined and some metastable structures are shown in Figure 10(b) and (c), respectively. P and O_i atoms are stable on each other's zigzag bond. Because the E_b of the $P-O_i$ pair is negative, P and O_i atoms do not bind.

3.3.5. Reaction of V and C_i-O_i

Figure 11(a) shows the calculated dependence of E_b on the number of Vsites from the C_iO_i pair. The most stable structure determined is shown in Figure 11(b). In the models of Vat sites No. 1, No. 4, and No.

10 shown in Figure 2(e), the C_i-O_i pair decomposes into C_s and O_i atoms. It is easily expected that V and C_i mutually annihilate, but it was also found that C_i of C_iO_i interact with V and disappears. When V is at No. 2, the C_i-O_i pair decomposes but C_i stays at the interstitial site as shown in Figure 11(c). When V is at No. 3, V disappears but the structure of C_i-O_i remains. The interactive distance of V and C_i-O_i is about 4 Å.

3.3.6. Reaction of P and C_i-O_i

Figure 12(a) shows the calculated dependence of E_b on the number of P sites from the C_iO_i pair. The most stable structure

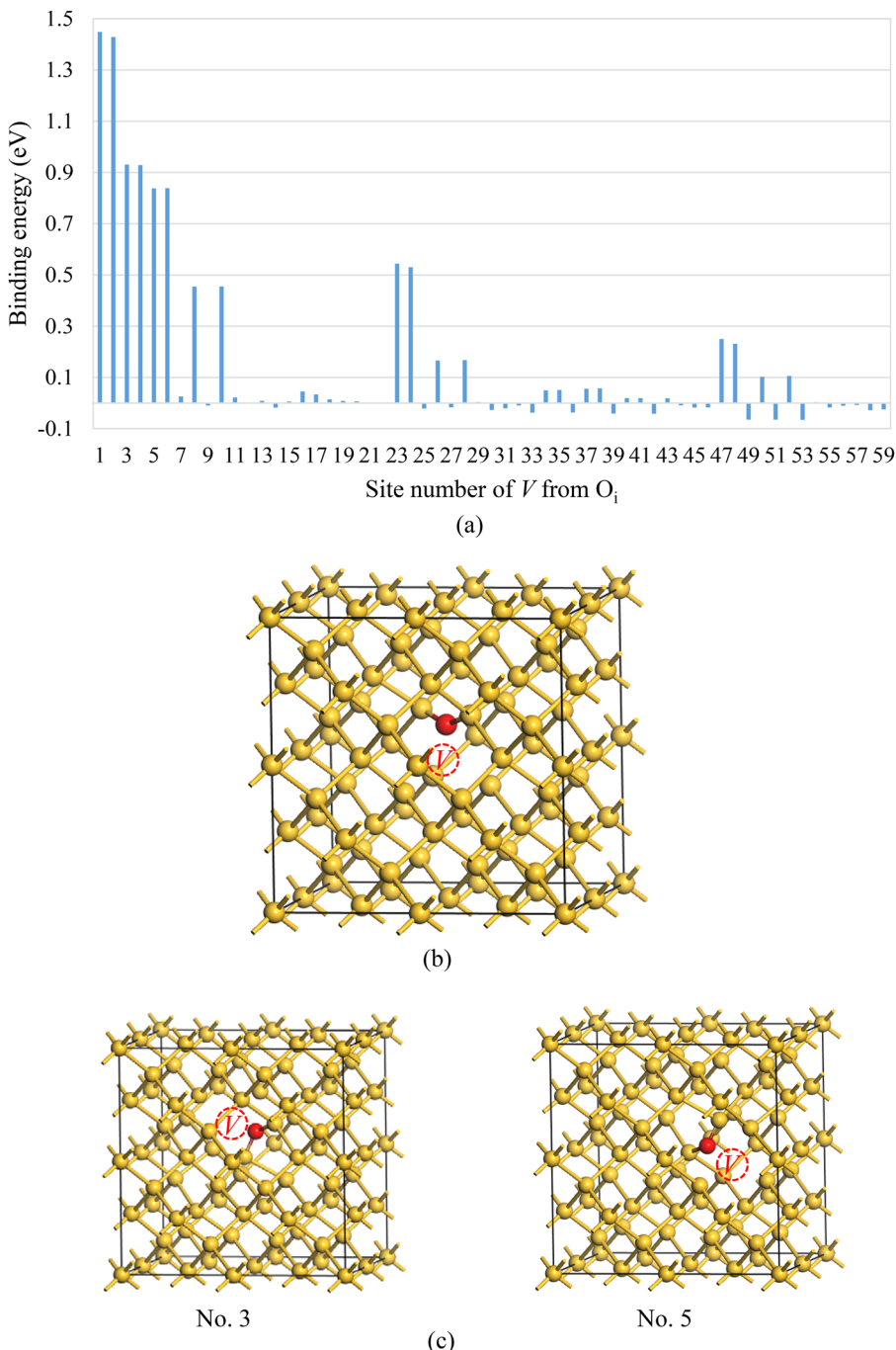


Figure 9. Calculation results about reaction of V and O_i . a) Dependence of E_b on the number of V sites from the O_i atom; b) most stable structure (No. 1 and No. 2) (gray/red sphere indicates C/O atom); and c) metastable structures.

determined is shown in Figure 12(b). In the most stable structure, $P-C_iO_i$ is divided into $P-C_i$ and O_i . The structures with negative E_b are shown in Figure 12(c). P and C_i-O_i are unstable on each other's zigzag bond as shown in Figure 12(d) without including sites No. 1 and No. 3. The combination of reactions of $P + C_i$ and $P + O_i$ are essential for the reaction of P and C_iO_i . In other words, P atom forms a complex with C_i atom, and not with O_i atom.

3.3.7. Reaction of V and C_i-C_s

Figure 13(a) shows the calculated dependence of E_b on the number of V sites from the C_iC_s pair. The most stable $V-C_iC_s$ pair (Figure 13b) is composed of V still existing at the 1st nearest neighbor site of C_iC_s . V and C_i-C_s pair are stable on each other's zigzag bond. There are two possible paths leading to the most stable structure: in the direction A (No. 15 \rightarrow No. 8 \rightarrow No. 2 \rightarrow No.

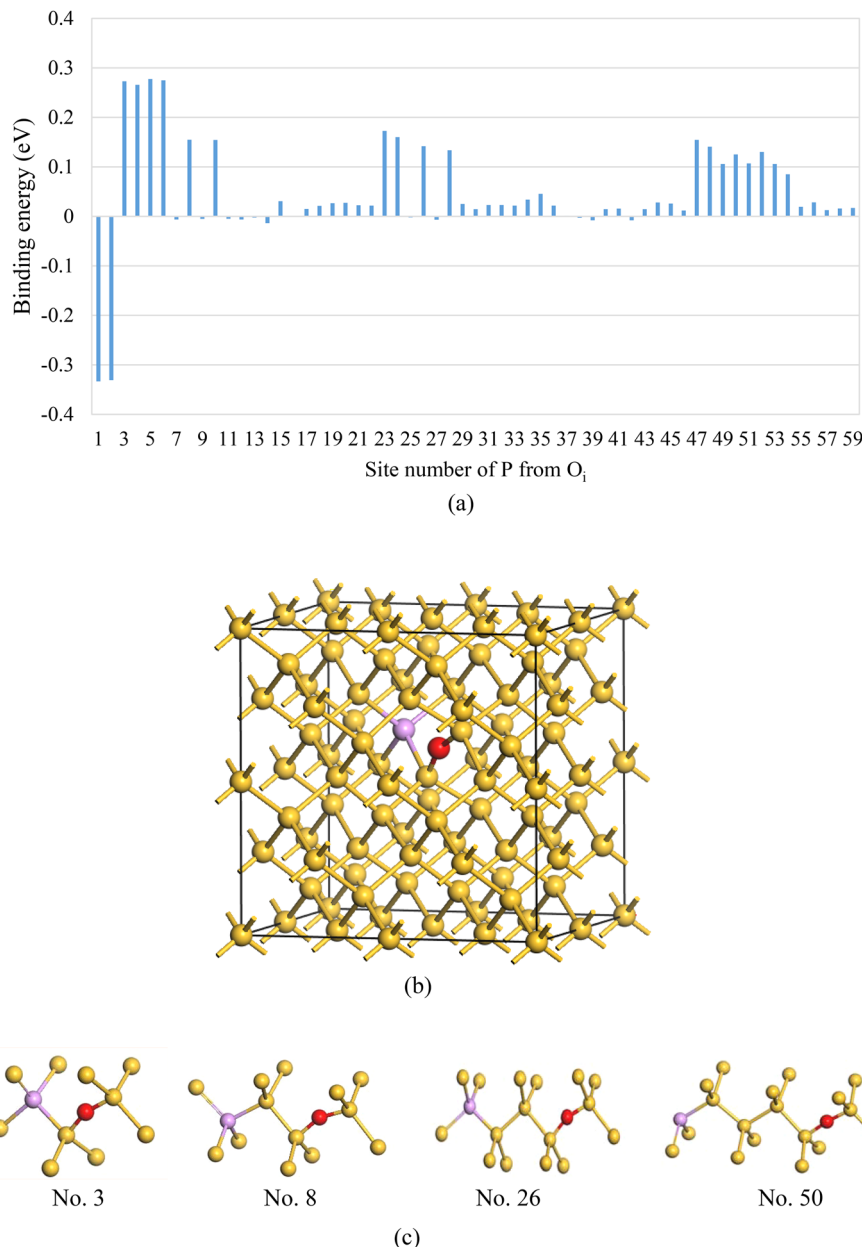


Figure 10. Calculation results about reaction of P and O_i . a) Dependence of E_b on the number of P sites from the O_i atom; b) most stable structure (No. 3) (red/purple sphere indicates O/P atom); and c) most stable and metastable structures.

1) and in the direction B (No. 16 → No. 9 → No. 3 → No. 1), although the direction A has more availability. Unlike the reactions of V and C_i (C_i-O_i), V remains without interacting with the C_i of the C_i-C_s defect. This is contrary to the expectation that V and C_i would disappear, which is a remarkable point to be found by simulation.

3.3.8. Reaction of P and C_i-C_s

Figure 14(a) shows the calculated dependence of E_b on the number of P sites from the C_i-C_s pair. The most stable structure determined and some metastable structures are shown in Figure 14(b). Stable P– C_iC_s pairs are composed of P existing at the zigzag bond in the direction B of the C_i-C_s defect. From Figure 14(a), the value of E_b is

positive even at the site with the least energy in this cell. This result indicates that the P and C_i-C_s are attracted over a distance. Figure 14(c) shows the effective charge of the C_i-C_s defect, which is negatively charged. Since P is a donor atom and positively charged, electrical interaction of P and C_iC_s pair is considered.

3.4. Summary of Calculations and Candidates to Affect Controllability of Lifetime

Figure 15 shows the atomic configuration of most stable complexes formed in each reaction. The calculated results can be summarized as follows:

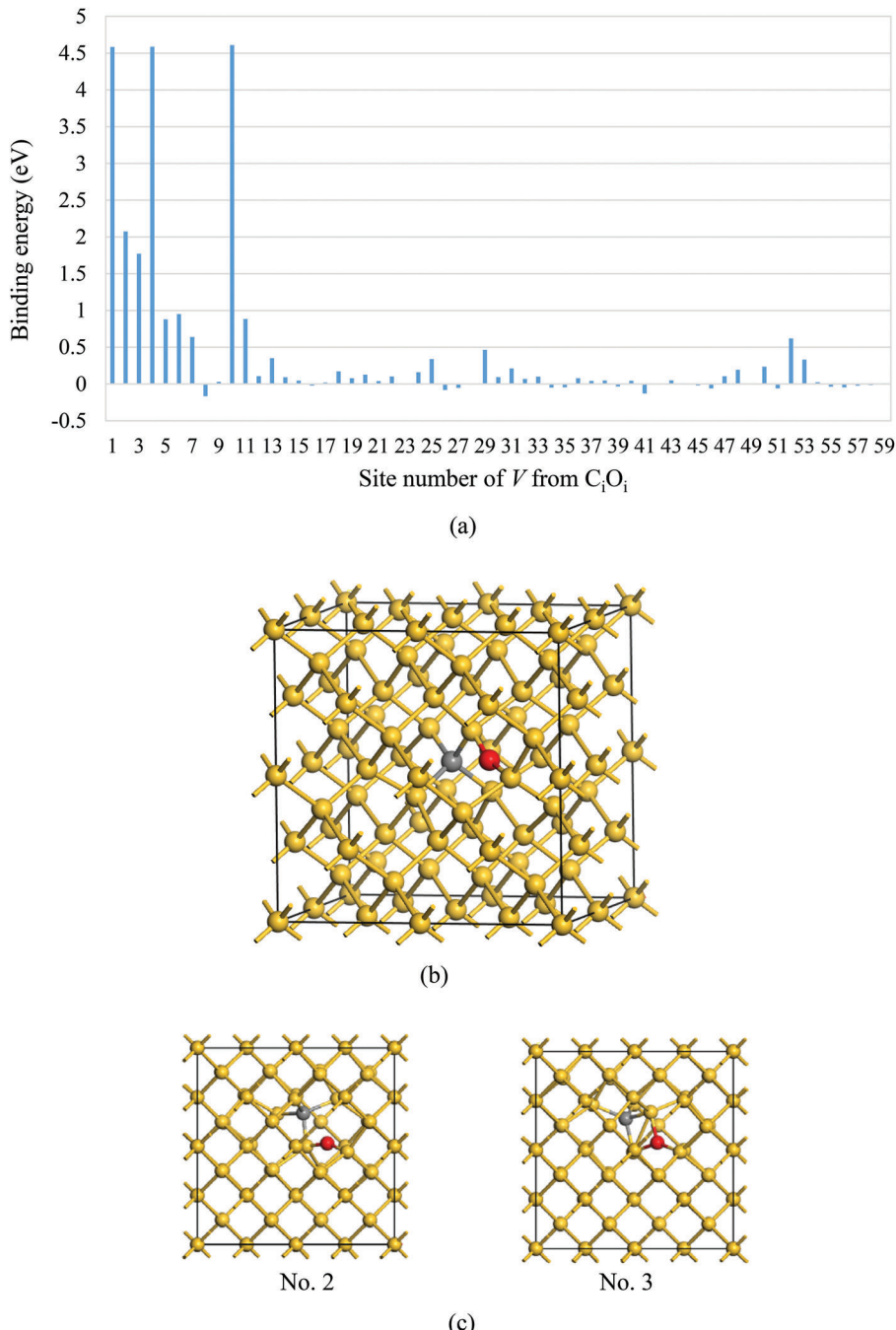


Figure 11. Calculation results about reaction of V and C_iO_i . a) Dependence of E_b on the number of V sites from the C_iO_i pair; b) most stable structure (No. 1, No. 4, and No. 10) (gray/red sphere indicates C/O atom); and c) metastable structures.

- 1) Lifetime-control defects ($V-V$ and $V-P$)
 - i) $V+V$: The $V-V$ pair is the most stable, and their interaction stays in the 1st neighbor site.
 - ii) $V+P$: The $V-P$ pair is the most stable, and their interaction is beyond the cell size of Si 64-atoms.
- 2) Complexes believed to interact with lifetime-control defects
 - i) C_s+I : C_s-I forms [100] dumbbell, which is the most stable.
 - ii) C_i+O_i : C_i and O_i atoms approach each other in the direction A and form the stable rhombic structure.
 - iii) C_i+C_s : C_i and C_s atoms form [100] dumbbell, which is the most stable.
- 3) Structural change of lifetime-control defects

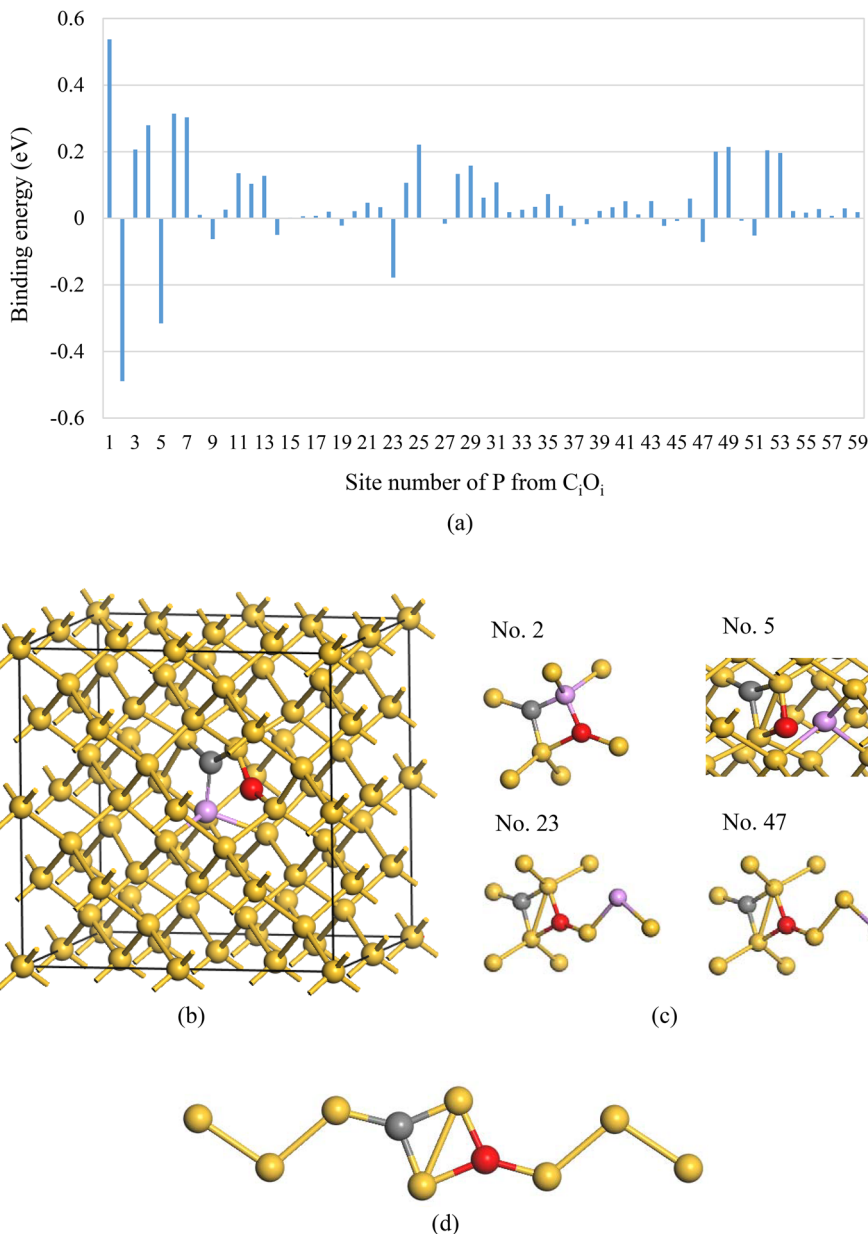


Figure 12. Calculation results about reaction of P and C_iO_i . a) Dependence of E_b on the number of P sites from the C_iO_i pair; b) most stable structure (No. 1) (gray/red/purple sphere indicates C/O/P atom); c) unstable structure; and d) zigzag bond including C_i-O_i (a P atom is at one of the substitutional sites).

- i) $V + C_i$: V and C_i atoms are annihilated and a C_s atom is formed.
- ii) $P + C_i$: P and C_i atoms form a $P-C_i$ dumbbell complex.
- iii) $V + O_i$: A $V-O$ complex is formed by an O_i atom binding two dangling bonds of V.
- iv) $P + O_i$: P and O_i atoms do not bind directly.
- v) $V + C_iO_i$: C_i of C_iO_i interacts with V, and C_iO_i decomposes into C_s and O_i atoms.
- vi) $P + C_iO_i$: C_i of C_iO_i interacts with P, and $P-C_iO_i$ decomposes into $P-C_i$ and O_i atoms.
- vii) $V + C_iC_s$: V remains at the 1st nearest neighbor of C_i-C_s .
- viii) $P + C_iC_s$: P remains at the 2nd nearest neighbor of C_i-C_s .

Table 2 summarizes the E_b of the most stable structures calculated by Si 64-atom and 216-atom cubic cells. E_b obtained by the previous studies are also summarized.^[4,7,11,12,22–30,41] It is found that, for (i) $C_s + I \rightarrow C_i$, (ii) $V + V \rightarrow V - V$, (iii) $C_i + O_i \rightarrow C_i - O$, (iv) $V + O_i \rightarrow V - O_i$, (v) $C_i + C_s \rightarrow C_i - C_s$, (vi) $P + V \rightarrow V - P$, (vii) $P + C_i \rightarrow P - C_i$, the calculated E_b well agreed with that obtained in the previous studies in the range of 0.3 eV. Referring to the E_b of Fe and B ($E_b = 0.68$ eV), which is often used for the critical value of effective gettering, the reactions above the bold line in Table 2 are likely to occur. In comparison with V and P, which are components of lifetime-control defects, the E_b of V with C_i , O_i , C_i-C_s , and C_i-O_i is relatively larger than that of P.

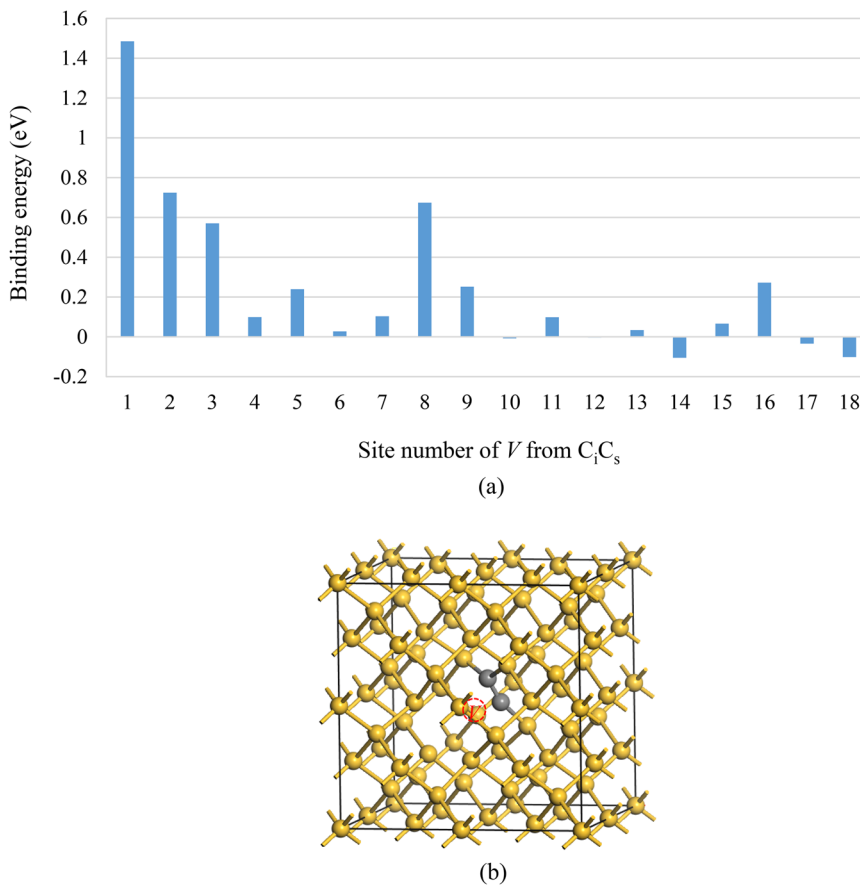


Figure 13. Calculation results about the reaction of V and C_i-C_s . a) Dependence of E_b on the number of V sites from the C_iC_s pair and b) most stable structure (No. 1) (gray sphere indicates C atom).

Table 2. Calculated E_b of most stable structures in Si 64- and Si 216-atom cubic cells.

Reaction	E_b [Si 64]	E_b [Si 216]	E_b [previous studies]
$V + C_i \rightarrow C_s$	5.44	5.58	
$V + C_i - O_i \rightarrow C_s + O_i$	4.58	4.68	
$C_s + I \rightarrow C_i (C_s - I)$	1.61	1.42	Cal) 1.3 ^[12] , 1.5 ^[26] , 1.56 ^[24]
$V + V \rightarrow V - V$	1.52	1.81	Cal) 1.43 ^[7] , 1.75 ^[22] Exp) 1.5 ^[4,41]
$C_i + O_i \rightarrow C_i - O_i$	1.49	1.32	Cal) 1.7 ^[11]
$V + C_i - C_s \rightarrow V - C_i C_s$	1.48	1.16	
$V + O_i \rightarrow V - O_i$	1.45	1.57	Cal) 1.29 ^[27] , 1.48 ^[28] , 1.50 ^[29] , 1.70 ^[30]
$C_i + C_s \rightarrow C_i - C_s$	1.36	1.03	Cal) 1.45 ^[23]
$P + V \rightarrow V - P$	1.02	1.18	Cal) 1.01 ^[23] , 1.1 ^[12] , 1.2 ^[24,25]
$P + C_i \rightarrow P - C_i$	0.88	0.82	Cal) 0.93 ^[23]
$P + C_i - C_s \rightarrow P - C_i C_s$	0.73	0.58	
$P + C_i O_i \rightarrow P - C_i + O_i$	0.53	0.51	
$P + O_i \rightarrow P - O_i$	0.27	0.21	

E_b obtained by previous studies are also summarized.

Unit: eV.

E_b of Fe and B: 0.68 eV

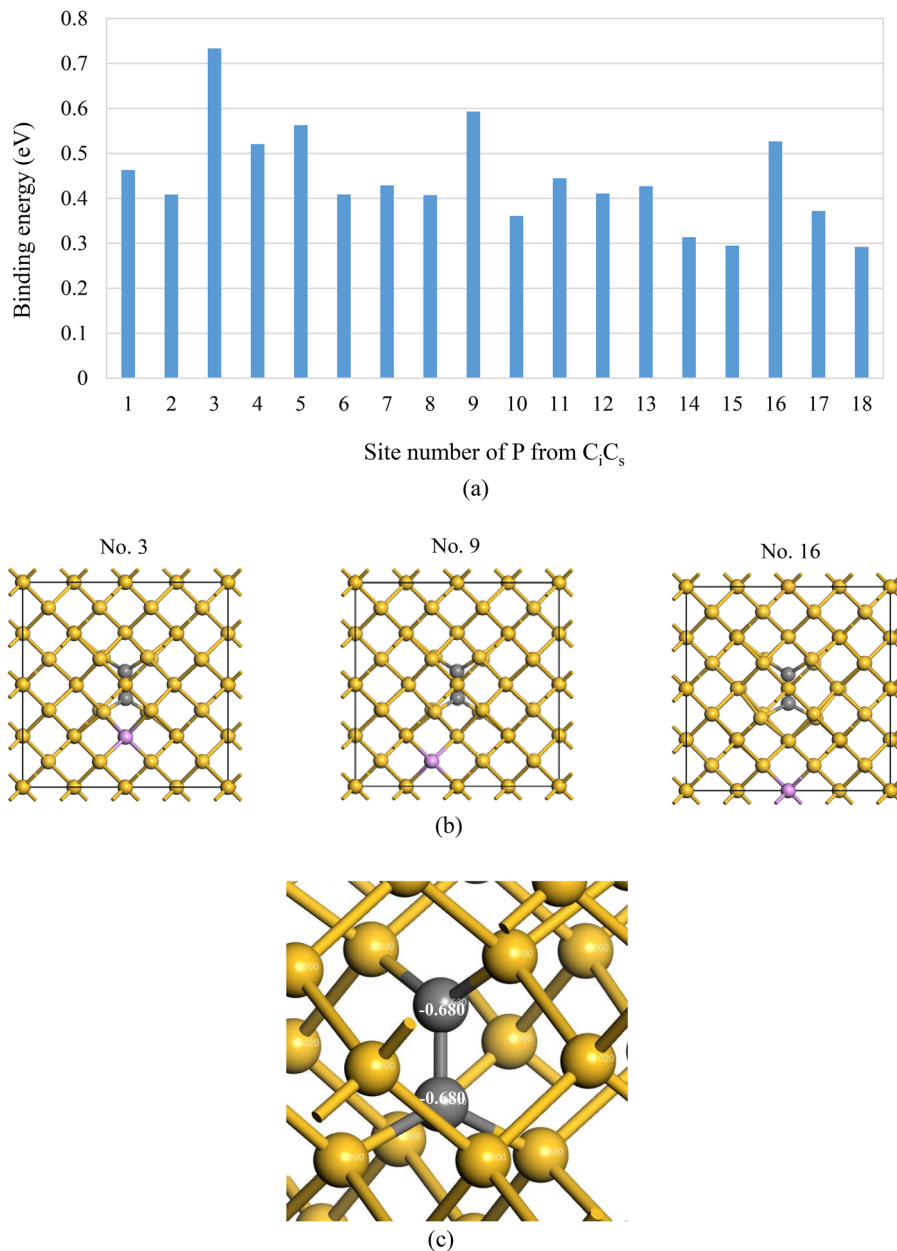


Figure 14. Calculation results about the reaction of P and C_i-C_s . a) Dependence of E_b on the number of P sites from the C_iC_s pair; b) most stable and metastable structures (gray/purple sphere indicates C/P atom); and c) effective charge of C_i-C_s .

Furthermore, it is found that not the C_i-C_s pair but the C_i atom and the C_i-O_i pair are the strong candidates to affect controllability of lifetime by interacting with V composed of lifetime-control defects. That is, the disappearance of deep levels of lifetime-control defects will extend the carrier lifetime by using the reaction of $V+C_i \rightarrow C_s$ and $V+C_iO_i \rightarrow C_s+O_i$ (independent C_s and O_i atoms do not form deep levels). The E_b of these reactions is very large so these reactions are likely to occur. This conclusion improves our understandings of the reactions that effect lifetime limiting defects.

The interactions of V-V (V-P) with C_i and C_i-O_i must be studied with a focus on the change of deep levels of lifetime-control defects in the near future.

4. Conclusion

To understand the in-activation of deep energy levels of lifetime-control defects (V-V pair and V-P pair) in P doped n-type Si crystals for IGBT, DFT calculations were performed to the following behaviors related to the lifetime-control defects:

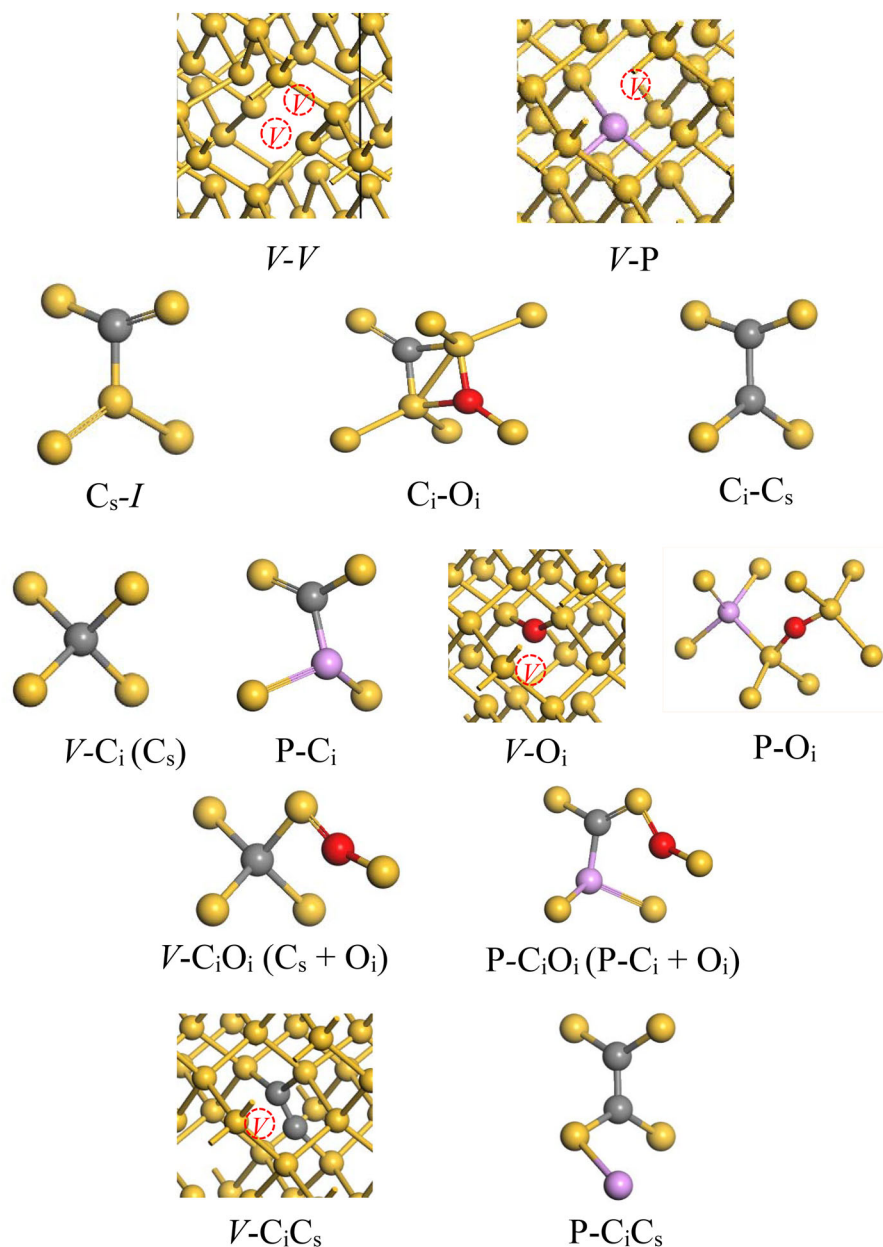


Figure 15. Most stable structures formed in each reaction.

- 1) Formation behavior of lifetime-control defects such as V–V and V–P.
- 2) Formation behavior of complexes ($C_s + I$, $C_i + O_i$, $C_i + C_s$) believed to interact with lifetime-control defects.
- 3) Structural change of lifetime-control defects ($P + C_i$, $P + O_i$, $V + C_i$, $V + O_i$, $P + C_iO_i$, $P + C_iC_s$, $V + C_iO_i$, $V + C_iC_s$).

The main results are summarized in Figure 15 and Table 2. Comparing V and P , which are components of lifetime-control defects, the E_b of V with C_i , O_i , C_i-C_s , and C_i-O_i is relatively larger than that of P . Furthermore, instead of the C_i-C_s pair, C_i and C_i-O_i pair are strong candidates to affect the controllability

of lifetime by interacting with V composed of lifetime-control defects. That is, the disappearance of deep levels of lifetime-control defects will extend the carrier lifetime by using the reaction of $V + C_i \rightarrow C_s$ and $V + C_iO_i \rightarrow C_s + O_i$.

Acknowledgments

This work was partially supported by JSPS KAKENHI grant Number 16K04950.

Conflict of Interest

The authors declare no conflict of interest.

Keywords

density functional theory, lifetime-control defect, power device, silicon crystals

Received: July 31, 2018
Revised: December 26, 2018
Published online:

- [1] T. Minato, K. Takano, A. Kiyo, in Proceedings of 29th International Conference on Defects in Semiconductors (ICDS) **2017**, TuA2-11.
- [2] T. Sugiyama, M. Yamazaki, A. Tanida, F. Niwa, T. Kanata, in Proceedings of the Forum on the Science and Technology of Silicon Materials **2010**, 206 and references therein.
- [3] G. D. Watkins, J. W. Corbett, *Phys. Rev.* **1964**, 134, A1359.
- [4] G. D. Watkins, J. W. Corbett, *Phys. Rev.* **1965**, 138, A543.
- [5] K. Sueoka, E. Kamiyama, J. Vanhellemont, *J. Appl. Phys.* **2013**, 114, 153510 and references therein.
- [6] N. Ganagona, L. Vines, E. V. Monakhov, B. G. Svensson, *J. Appl. Phys.* **2014**, 115, 034514.
- [7] E. Kamiyama, K. Sueoka, J. Vanhellemont, *Phys. Stat. Sol. B* **2014**, 251, 2185.
- [8] L. F. Makarenko, F. P. Korshunov, S. B. Lastovski, L. I. Murin, M. Moll, *Solid State Phenomena* **2010**, 156, 155.
- [9] M. T. Asom, J. L. Benton, R. Sauer, L. C. Kimerling, *Appl. Phys. Lett.* **1987**, 51, 256.
- [10] L. W. Song, X. D. Zhan, B. W. Benson, G. D. Watkins, *Phys. Rev. B* **1990**, 42, 5765.
- [11] L. I. Khirunenko, M. G. Sosnin, Yu. V. Pomozov, L. I. Murin, V. P. Markevich, A. R. Peaker, L. M. Almeida, J. Coutinho, V. J. B. Torres, *Phys. Rev. B* **2008**, 78, 155203.
- [12] K. Sueoka, E. Kamiyama, P. Śpiewak, J. Vanhellemont, *ECS J. Solid State Sci. Tech.* **2016**, 5, P3176.
- [13] H. Wang, A. Chroneos, D. Hall, E. N. Sgourou, U. Schwingenschlögl, *J. Mater. Chem. A* **2013**, 1, 11384.
- [14] A. Chroneos, C. A. Londos, *J. Appl. Phys.* **2010**, 107, 093518.
- [15] H. Wang, A. Chroneos, C. A. Londos, E. N. Sgourou, U. Schwingenschlögl, *Appl. Phys. Lett.* **2013**, 103, 052101.
- [16] H. Wang, A. Chroneos, C. A. Londos, E. N. Sgourou, U. Schwingenschlögl, *Sci. Rep.* **2014**, 4, 4909.
- [17] A. Chroneos, E. N. Sgourou, C. A. Londos, U. Schwingenschlögl, *Appl. Phys. Rev.* **2015**, 2, 021306.
- [18] K. Kobayashi, S. Yamaoka, K. Sueoka, *J. Cryst. Growth* **2017**, 474, 110.
- [19] H. Koyama, K. Sueoka, *J. Cryst. Growth* **2017**, 463, 110.
- [20] K. Sueoka, K. Nakamura, J. Vanhellemont, *J. Cryst. Growth* **2017**, 474, 89.
- [21] F. Zirkelbach, B. Stritzker, K. Nordlund, J. K. N. Lindner, W. G. Schmidt, E. Rauls, *Phys. Rev. B* **2011**, 84, 064126.
- [22] E. Kamiyama, J. Vanhellemont, K. Sueoka, *AIP Adv.* **2015**, 5, 017127.
- [23] S. Shirawawa, K. Sueoka, T. Yamaguchi, K. Maekawa, *Mater. Sci. in Semiconductor Proc.* **2016**, 44, 13.
- [24] B. Sahli, K. Vollenweider, W. Fichner, *Phys. Rev. B* **2009**, 80, 075208.
- [25] H. Bracht, A. Croneos, *J. Appl. Phys.* **2008**, 104, 076108.
- [26] J. Zhu, T. Diaz de la Rubia, C. Mailhot, *Mater. Res. Soc. Symp. Proc.* **1997**, 439, 59.
- [27] K. Sueoka, *ECS Trans.* **2006**, 3, 71.
- [28] G. Kissinger, J. Dabrowski, D. Kot, V. Akhmetov, A. Sattler, W. Von Ammon, *J. Electrochem. Soc.* **2011**, 158, H343.
- [29] V. J. B. Torres, J. Coutinho, R. Jones, M. Barroso, S. Öberg, P. R. Briddon, *Phys. B* **2006**, 376, 109.
- [30] R. A. Casali, H. Rücker, M. Methfessel, *Appl. Phys. Lett.* **2001**, 78, 913.
- [31] A. Yamada, K. Sueoka, *ECS J. Solid State Sci. Tech.* **2017**, 6, P125.
- [32] D. Vanderbilt, *Phys. Rev. B* **1990**, 41, 7892.
- [33] J. Perdew, K. Burke, M. Ernzerhof, *Phys. Rev. Lett.* **1996**, 77, 3865.
- [34] S. J. Clark, M. D. Segall, C. J. Pickard, P. J. Probert, K. Refson, M. C. Payne, *Z. Kristallogr.* **2005**, 220, 567.
- [35] G. Kresse, J. Furthmüller, *Phys. Rev. B* **1996**, 54, 11169.
- [36] T. Fischer, J. Almlöf, *J. Phys. Chem.* **1992**, 96, 9768.
- [37] H. Monkhorst, J. Pack, *Phys. Rev. B* **1976**, 13, 5188.
- [38] A. Chantre, L. C. Kimerling, *Appl. Phys. Lett.* **1986**, 48, 1000.
- [39] G. D. Watkins, *Defects in Semiconductors 15, Materials Science Forum* (Ed: G. Ferenczi). Trans Tech, Switzerland **1989**, Vol. 38-41, p. 39.
- [40] E. Gürer, B. W. Benson, G. D. Watkins, *Defects in Semiconductors 16, Materials Science Forum* (Eds: G. Davies, G. G. DeLeo, M. Stavola). Trans Tech, Switzerland **1992**, Vol. 83-87, p. 339.
- [41] J. W. Corbett, *Electron Radiation Damage in Semiconductors and Metals*. Academic, New York **1996**, and refs. therein.